PUBLICATIONS OF THE ASTRONOMICAL SOCIETY OF THE PACIFIC
102: 1433–1441, December 1990

THE CERRO TOLOLO INTER-AMERICAN OBSERVATORY INFRARED SPECTROMETER

D. L. DEPOY, BROOKE GREGORY, JONATHAN ELIAS, ANDRÉS MONTANÉ, GABRIEL PÉREZ, AND ROGER M. SMITH

Cerro Tololo Inter-American Observatory, National Optical Astronomy Observatories,* Casilla 603, La Serena, Chile

Received 1990 July 27

ABSTRACT

An infrared spectrometer (IRS) is available for use at the Cerro Tololo Inter-American Observatory. The instrument has a slit of modest length and a selection of gratings that allow resolutions ($\lambda/\Delta\lambda$) from ~ 150 to ~ 3000 over the wavelength range covered by its photovoltaic InSb array: 0.9 μm to 5 μm. The design and operating characteristics of the IRS are described, and observing procedures and data-reduction techniques are outlined for potential users.

Key words: instrumentation–infrared–spectrometers

1. Introduction

The recent widespread availability of infrared arrays for astronomical use has led to enormous gains in the efficiency and sensitivity of infrared observations. To date, imaging systems using these arrays have been most common, due to their relative ease of design and construction (cf. Gatley, DePoy, and Fowler 1988). Spectrometers, however, are also obvious applications of arrays: The multiplex advantage of many wavelength samples and the integrating nature of the arrays improve sensitivity over previously available instruments by several orders of magnitude.

This paper describes the Cerro Tololo Infrared Spectrometer (IRS), a multipurpose, cooled-grating spectrometer for the CTIO 4-m and 1.5-m telescopes. It is designed to function over the near-infrared spectral range covered by InSb detectors, from 0.9 μm to 5.0 μm, at spectral resolutions up to a few thousand. This paper gives an account of the design and engineering aspects of the spectrometer that may be of interest to instrumentalists and provides a general description for potential users.

The instrument was originally built for an eight-element, one-dimensional array, which was recently replaced by a 2-D detector. We describe the IRS in its present form only. Although the instrument was designed with the possibility of such an upgrade in mind, the result is not necessarily optimal for the present detector.

2. Optical Design

The spectrometer was designed to admit a full stellar seeing disk on the 4-m telescope working with the *f*/33 chopping secondary and to provide a spectral purity of about 1000 with a grating blazed at 30 degrees. For a 2-mm slit and a reasonable diffraction angle (20 degrees), this calls for a collimated beam diameter of about 50 mm and a collimator focal length of 1600 mm. The camera focal length was chosen to image the slit onto a single detector (0.25 mm wide) in the original eight-element array. The current 62 × 58 element Santa Barbara Research Corporation (SBRC) array has square pixels on 0.076-mm centers. The optics are unchanged in the current instrument except that the preslit field lens now has slightly greater demagnification. Although the slit width corresponding to 2 pixels on the detector is now only 1.″6–2.″0 on the 4-m telescope, experience shows that this still gives good spectrophotometric performance (see Section 6.3). Table 1 shows the resulting scales on the two telescopes. Because the telescope *f*-ratios are not identical, the scale is not exactly proportional to the inverse of the aperture.

An optical layout of the spectrometer is shown in Figure 1. With the telescope at the zenith, the optical table is vertical. Light from the telescope is directed by a warm 45-degree dichroic mirror to the cold 45-degree entrance mirror in the cryostat. From then on the optical axes of

TABLE 1
Image Scales

Scale	Telescope	
	4 m	1.5 m
at slit:	2.01	5.94 arcsec mm^{-1}
at detector:	0.81	2.38 arcsec $pixel^{-1}$

*Operated by the Association of Universities for Research in Astronomy, Inc., under cooperative agreement with the National Science Foundation.

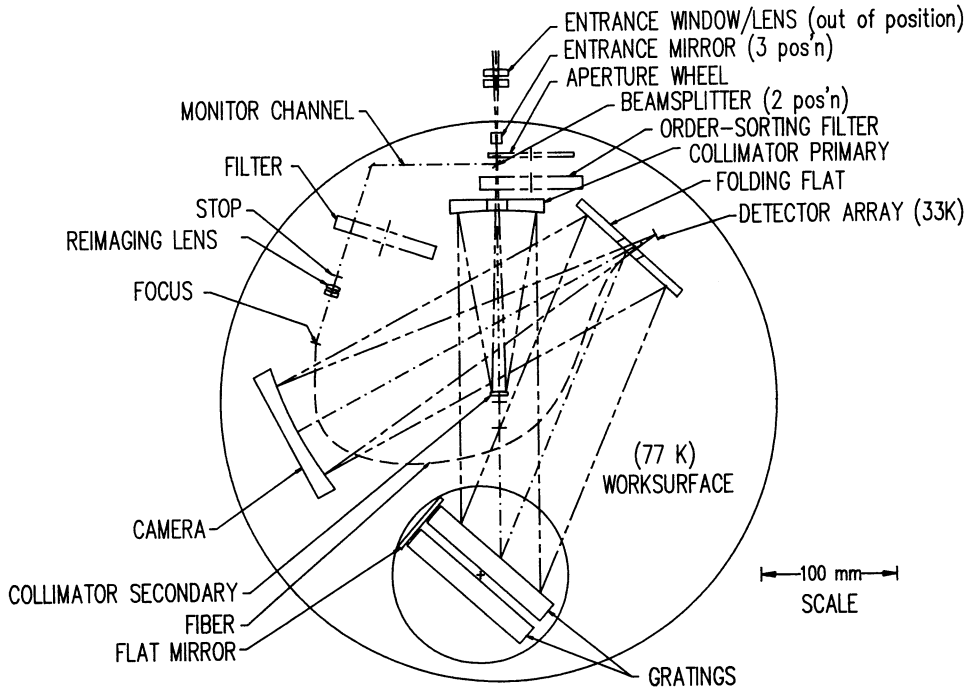

FIG. 1—Optical layout of the spectrometer; the monitor channel is not used.

the system are parallel to the work surface.

2.1 *Entrance Optics*

The entrance window of the dewar is an achromatic BaF_2/LiF doublet which, acting together with the collimator secondary, produces an image of the telescope secondary at the position of the collimator primary, where the principal stop of the system is placed. Because light that is not absorbed by the black stop is directed toward the interior of the spectrometer, it is not an ideal cold stop, and the light scattered from its surface represents a potentially important source of background radiation in the dewar. To diminish the solid angle on the sky which actually reaches this surface, additional baffles are located in front of the hole of the collimator primary.

In addition to assisting in baffling the out-of-beam radiation, the entrance window lens is essential to make the Cassegrain collimator function efficiently, reducing the footprint of the radiation for the full field of the entrance slit on all of the further optical surfaces. The full field shift on the camera of the central ray is reduced from 25 to 1 mm by the field lens. For the small detector used here, the vignetting by the central obstructions in the spectrometer is effectively zero.

The entrance lens produces a demagnification of the telescope focal plane on the aperture of 1.35 and transforms the beam f-ratio from $f/33.0$ to $f/24.4$.

There are two other windows on the dewar whereby light can reach the slit: a window on the top of the dewar used for diagnostics and a window on the back for admitting light from the comparison sources. The latter is a BaF_2 lens which images the output hole of the integrating cavity of the comparison light source onto the slit. The remotely operated entrance mirror mover internal to the dewar has two mirrors and one open position permitting light to reach the slit from each of the three windows.

2.2 *Cassegrain Collimator*

The collimator is of Dall-Kirkham (spherical secondary) design. The overall focal length is 1584 mm. The cold-stop diameter on the primary has a diameter of 66.0 mm which corresponds to $f/24$.

2.3 *Gratings, Imaging Mirror*

The gratings are gold overcoated standard replicas from Milton Roy on Pyrex substrates. The gratings are mounted with the rulings and rotation axis normal to the work surface. The incident and diffracted beams are parallel to the work surface, with a total diffraction angle of 23.5 degrees. Two gratings can be mounted, back to back, on a rotating grating table moved by a worm gear and stepping motor. The gratings currently in use are listed in Table 2.

The grating table also carries a flat mirror which permits imaging in undispersed light. This is valuable in locating and centering faint objects. Because the flat mirror is not on the grating table axis there is some vignetting (83% throughput) of the beam.

2.4 *Folding Flat, Camera*

A flat mirror, perforated in the center, puts the beam on the axis of the camera, which is a simple parabola of 300-mm focal length. The flat can be manually, not

TABLE 2

Gratings

Grating [l mm^{-1}]	Blaze [μm]	Blaze [degrees]	Bands	Resolution[a]
12	6.7	2.3	I,J,L	159
75	4.5	10.0	I,J,H,K,L	650
210	4.2	26.	I,K,M	1905
632	2.4	51.0	J,K	3870

[a]Resolution: $\lambda/\Delta\lambda$, for two pixels, near blaze

remotely, tipped a small amount to adjust the image of the slit on the array in the cross-dispersion direction.

2.5 *Detector Array*

The current detector is a 62 × 58 element InSb direct readout (DRO) array manufactured by Santa Barbara Research Corporation. The longer dimension is in the direction of dispersion. The pixels are square, on a 76-μm grid (see Section 5.1).

3. Mechanical Design

The detector dewar is a squat cylinder with a horizontal axis of symmetry when the telescope points at the zenith. This design preserves the mechanically simplifying advantages of cylindrical construction, while providing a large flat area (perpendicular to the cylinder axis) for mounting the optical train. Figure 2 shows a simplified schematic of the primary components of the instrument dewar. The cryogen flasks are filled with liquid nitrogen. The inner dewar may be pumped on to cool it further to about 50 K (as was necessary with the original detector). The cryocooler cools only the detector.

The dewar is mounted on the side of a box which houses a 45-degree dichroic and a television acquisition and guiding system. Thus, the dewar is "side looking" with the principal entrance window on the flat circular cover of the dewar vessel.

3.1 *Dewars, Mechanical Support*

Virtually all of the structural components of the instrument are made of aluminum or, where low thermal conductivity is desired, of G10-CR fiberglass. In addition to being economical to acquire and fabricate, these materials are well matched to each other in thermal contraction and both have excellent strength-to-weight ratios. Though copper would have a higher thermal conductivity than aluminum, the thermal loads on the low-temperature portions of the dewar are low and it is easy to achieve the required isothermality with aluminum.

All of the thermally insulating mechanical support of the cold innards of the dewar is provided by two short, large-diameter, open cylinders of fiberglass located

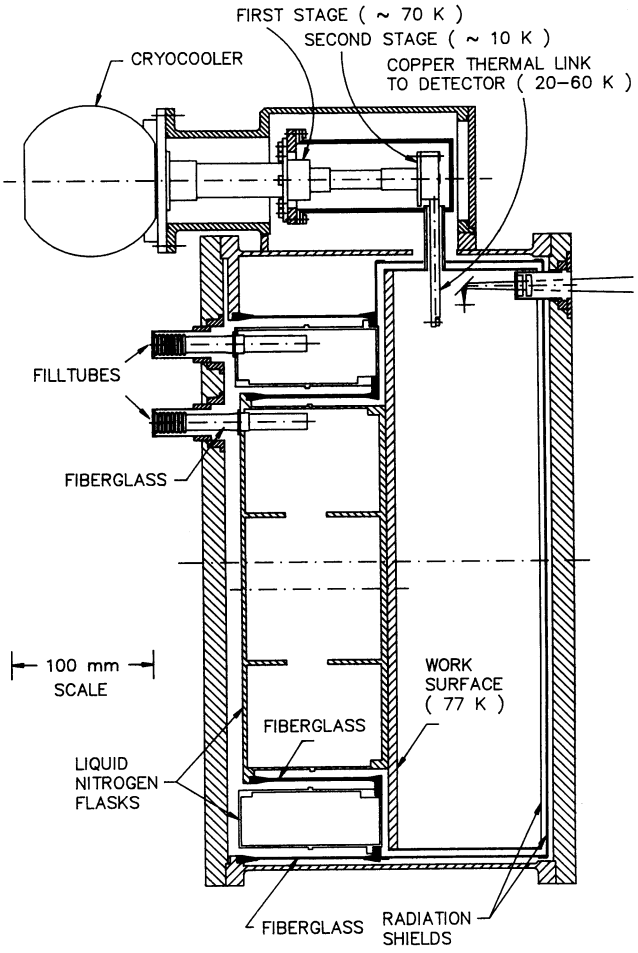

FIG. 2–Dewar construction.

around the two cryogen flasks. One cantilevers the inner, cylindrical flask off the outer, annular one. The other joins the outer dewar to the back flange of the vacuum vessel and supports the entire weight of the cooled part of the instrument. The outer and inner cylinders have wall thicknesses of 0.031 and 0.062 inch, respectively. The fiberglass cylinders are epoxied[1] into hoops of aluminum which are in turn bolted to the end rims of the dewars. The shear stiffness of the low-aspect-ratio cylinder is extremely high so the overall stiffness of the structure is excellent. Based on measured deflections, the estimated worst-case tilt with 90-degree reorientation of the instrument is 1.6×10^{-5} rad, approximately five parts in 10^4 of the beam diameter.

Note that the thermal gradients along the cylinders of fiberglass cause them to become slightly conical without developing large internal stresses, as they accommodate the thermal contraction of the dewars. G10 fiberglass and aluminum have similar thermal expansion coefficients, so

[1]Crest 3170 epoxy, manufactured by Crest Products Corp. (2000 Susan Street, Santa Ana, CA 92704).

there is virtually no thermally induced stress in the joints.

The outer, annular dewar was machined in two halves from solid material and welded at the midplane. The inner dewar was fabricated similarly, but with the difference that deep webs of material were left on the faces inside of the dewar to stiffen them and to provide greater surface area for thermal transport from the (possibly solid) nitrogen cryogen it contains.

Two radiation shields, connected to the inner and outer dewars, respectively, each completely surround the optical volume. The outer shield reduces light leakage, decreases heat input to the inner dewar, and ensures that the inner radiation shield is everywhere sufficiently cold to suppress emission.

The orientation of the dewar minimizes spillage from the liquid-nitrogen flasks. The orientation of the dewar and the concentric arrangement of the flasks makes horizontal fill tubes almost obligatory. The dewars are easily filled, however, by squirting the nitrogen into the fill tubes from a pressurized nitrogen storage dewar. The cryogen fill tubes (Fig. 2) consist of filament-wound fiberglass tubes epoxied between the dewar and short sections of stainless-steel bellows. The bellows provide stress relief and accommodate thermal contraction.

An incidental benefit of this design is that the inner dewar, the work surface, and its radiation shield form an electrically isolated Faraday cage which can be electrically referenced to the outside world in a controlled way.

3.2 *Work Surface, Optical Components, Optical Mounts*

All of the cold optical components are mounted on a flat plate of aluminum which is bolted to a raised outer rim on the inner dewar flask. All of the mirrors and grating blanks are Pyrex. To ensure reproducible optical alignment with thermal cycling, some pains were taken in the design of the mounts for the Pyrex components to provide for thermal expansion while avoiding hysteresis. Where possible the expansion was accommodated by flexure rather than by sliding. For example, in the case of the mirror cells the radial and axial definition is provided by a circular frame of spring fingers which holds the front edge of the mirrors. The axial loading against the frame is provided by spring-loaded plungers acting on the rear surface (without exerting additional radial forces).

At thermal equilibrium there will be no stresses at interfaces between aluminum components, but during cool down it is possible for stresses to develop that would cause the components to "walk". Consequently, all component mounts were pinned to the work surface and, with one exception, no large surfaces were bolted together. The exception is the joint between the work surface and the inner dewar.

3.3 *Alignment*

Because of differential thermal contraction between Pyrex and aluminum, the instrument will change its state of focus with temperature. Collimation should, however, be maintained because of the symmetry of the mounts and the precautions mentioned above. Thus, alignment of the instrument can be largely done at room temperature, requiring only a focus adjustment on cooling. To permit final alignment at low temperatures, all of the essential adjustments (and several others as well) were made available in the cooled instrument via a special set of perforated radiation shields and vacuum cover, to permit access with special screwdrivers to the control screws on the several elements that required adjustment. These fixtures are used for alignment only, since they emit and admit too much stray radiation for use at the telescope. The adjustments are all arranged so that they can be adjusted with a screwdriver perpendicular to the work surface. The screwdrivers have simple fiberglass shafts sealed with o-rings at the vacuum cover. Each adjustment is provided with a locking screw so that the adjustments will not be disturbed after setting.

On thermal cycling, the optical alignment is maintained adequately except in one respect: The image of the slit on the detector is shifted by a few pixels. To cope with this shift, the adjuster for the tilt of the folding flat was included in the observing configuration of the instrument. (Smaller shifts in the dispersion direction are also observed, but these are simply corrected by the grating calibration procedure.)

3.4 *Cryocooler*

A CTI model 22 cryocooler is used to cool the SBRC InSb array detector to the temperature required for low dark current. The cryocooler second stage reaches a temperature of about 10 K. The detector mount is connected via a cold finger of copper to this stage (Fig. 2). After discovering and eliminating a resonance in one of the optical mounts, the vibration of the cryocooler has been found to produce no measurable effect on the images.

3.5 *Detector Mount*

The leadless chip carrier holding the detector is held in a socket which is in turn mounted on a sandwich of materials to provide mechanical support and thermal and electrical connection to the chip (Fig. 3). A thinned (0.25-mm) fiberglass printed circuit board is bonded to the face of an aluminum structure that carries heaters and the thermal strap to the second stage of the cryocooler. The copper printed circuit, cooled by conduction through the thin fiberglass layer, carries short tracks for the input leads. This and the aluminum cover-plate/baffle, which presses the chip carrier against the spring contacts, provide the primary cooling paths for the detector. The resulting structure has a very short thermal time constant and a low thermal mass. The circuit-board assembly is thermally isolated from the bracket to the work surface by a thin-walled fiberglass tube. A temperature sensor on the chip and heaters on the aluminum thermal ground

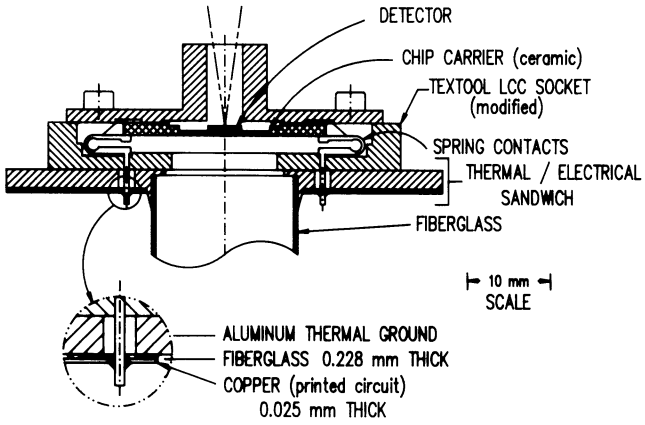

FIG. 3–Detector mount.

plane provide for temperature control. The detector is currently operated at about 35 K. Adequate control is obtained over a range of 20 K–60 K.

3.6 *Motorized Actuators*

With the exception of the single, manual adjustment of the folding-flat tilt described above (which only needs to be made during the instrument setup), all other spectrometer motions are made by stepper motors under computer control. The motions are filter wheels (2), aperture wheel, entrance mirror selector, beam splitter selector, and grating drive. With the exception of the grating drive, discussed below, the drive shafts (G10 fiberglass tubes) all pass through the rear cover of the dewar and the annular space around the cryogen flasks. To prevent light leaks around the shafts, they pass through narrow clearance holes in the outer radiation shield and are baffled with labyrinths and felt washers where they pass through the work surface. The vacuum seals are single o-ring seals on polished, hardened steel shafts.

3.7 *Grating Drive*

Because of the orientation of the grating axis and a desire to drive the grating as directly as possible, the grating drive motor shaft was brought into the dewar radially. The grating table is mounted on a commercial 360-tooth gear wheel driven by a worm. The worm was mounted in a special housing that permits the worm to move radially with respect to the wheel, but eliminates endplay and keeps the worm at the midplane of the wheel. To eliminate backlash, the housing and worm were loaded radially against the wheel with a spring. A Teflon-filled delrin worm provides smoother, lower-friction performance than does a stainless-steel worm.

The grating drive has an encoder on the motor shaft to confirm that the grating motions have been accomplished and to check the reproducibility of motor positions at a substep level. The motor positioning is reproducible to approximately 0.1 step. There are 72,000 steps to rotate the table through 360 degrees. With the SBRC array working at a blaze angle of 30 degrees (corresponding to a two-pixel resolution of about 2000) this corresponds to 1.5 motor steps per pixel. Friction and windup of the shaft between the motor and the gear degrade the resettability of the gear to about 0.3 step.

3.8 *Gimbal*

The dewar is mounted on the guider/acquisition box by means of a two-axis gimbal that permits fine adjustment of the instrument beam direction with respect to the telescope axis. The gimbal axes are arranged to pass through the center of the slit so the adjustment can be made without shifting the field of view during the adjustment.

4. Data Acquisition and Instrument Control

Control of the array and acquisition of data are accomplished by a FORTH system running in an LSI/11 developed at NOAO for the SBRC arrays (Zizzo and Slaughter 1986; Fowler *et al.* 1988; Fowler and Gatley 1990). The computer is interfaced via a DRV11 DMA interface to a bit-slice microprocessor providing control waveforms to the detector, video card, and analog-to-digital converter. The DRV11 is also used to send the data back to the FORTH 11 system where it can be displayed, analyzed, and stored on disk. There is also a link from the LSI/11 to the telescope data-reduction computer, a SUN work station running IRAF[2]. The mechanical control of the spectrometer itself is handled independently by the IRSPHOT program running in a DG Eclipse S/130.

A major project is underway to replace the array and instrument control system with one which more fully integrates data acquisition, spectrometer control, and data reduction.

5. Observing Procedures and Data Reduction

The IRS is capable of a wide range of scientific projects, so a detailed description of all applicable observing procedures and data-reduction techniques is impossible. However, generally pertinent methods are outlined in this section. Reduction of IRS data at CTIO is done using IRAF, but the procedures discussed below should be adaptable for use with other image-analysis software. They are similar to the methods used to obtain and reduce long-slit spectroscopic data taken using a CCD detector, although considerable differences exist when working with the IRS and its SBRC InSb array in the infrared: relatively small slit and restricted spectral coverage, unstable dark current and bias level and higher proportion of bad pixels, and large and variable sky emission and absorption.

A general method of reducing IRS data is to subtract

[2]IRAF is distributed by National Optical Astronomy Observatories, which is operated by the Association of Universities for Research in Astronomy, Inc., under cooperative agreement with the National Science Foundation.

an appropriate sky frame, divide by a flat field, reduce the spectra to one-dimensional form (using, for example, the IRAF "apextract" routines; this step can also remove any residual sky line emission), and, finally, divide by reference and/or standard stars to cancel any atmospheric absorption features and provide flux calibration. The steps not already well documented within IRAF are discussed in more detail in the following sections.

The measurements required for proper data reduction by and large determine the correct observing procedures; these, too, are discussed in the following sections. Attention to a few details improves the quality of any IRS data. First, the spectrophotometric performance of the IRS depends most critically on careful and accurate placement of an object on the slit (see Section 6.3). Although no "slit-viewing" camera is available with the IRS, the detector array can be continuously read out and, using either the zero order of a grating or the mirror (Section 2.3) installed on the grating turntable, an object can be centered on the slit. We have encountered no difficulty centering objects as faint as $K = 14$ on the 4-m telescope while using this "movie" mode and the mirror. Next, the SBRC InSb array is slightly nonlinear, most noticeably above $\sim$ 10,000 ADU ($\sim$ half of the full-well depth). Therefore, integration times should be set to avoid a linearity correction. Note that the low read noise of the array ($\sim$ 80 electrons, see Section 6.1 and Fowler and Gatley 1990) makes any integration time longer than several minutes unnecessary, since nearly all measurements made with the IRS are background limited in this time. Finally, the wavelength calibration should be determined using the built-in calibration sources (argon and xenon discharge lamps; night-sky emission lines can also be used) observed before and after the target observations. This is especially important when very precise wavelength determination is desired, since the grating movements are not perfect (see Section 3.7; the grating position is repeatable to $\sim$ 0.3 pixel). Observing at wavelengths $\gtrsim$ 3 μm imposes other constraints. The background at 3.5 μm is nearly 1000 times greater than at 2.2 μm and continues to increase exponentially. Therefore, integration times are relatively short and many individual frames must be coadded per observations. The sensitivity of the IRS, because of the large background noise, is relatively low at longer wavelengths. For example, measuring a star with $K = 10$ is simple on the 1.5-m telescope, but a star with $L = 10$ takes $\sim$ 1 hour on the 4-m telescope to obtain $S/N \sim 5$ at low resolution.

5.1 *Sky Measurements*

The infrared sky is usually much brighter than the object being measured, and both the sky continuum and emission lines vary in intensity. Consequently, removal of the sky contribution from the data frames is necessary prior to subsequent data reduction. Despite the two-dimensionality of the (albeit small) slit, this is best done with independently observed sky frames, since apparently intrinsic device instabilities limit flat-field accuracy to $\sim$ 1% (see next section).

The sky observations should be interspersed among the object observations in a mode analogous to "beam switching" with single-channel photometers (e.g., obj-sky-sky-obj-etc.). We find that integrating as long as several minutes in the near-infrared (long enough to become background limited) poses no serious problem for accurate sky subtraction. The individual sky measurements should generally be made at slightly different positions on the sky and subsequently medianed or averaged using iterative rejection algorithms. This procedure eliminates the chance occurrence of a star in the "sky" frame and removes any cosmic-ray events and detector drift. It is also possible to move a small source along the slit on consecutive observations, constructing a sky afterward using the same median or averaging techniques and averaging the subsequently resulting one-dimensional spectra. This technique will improve the *S/N* possible in a given time but must be used with caution due to the small size of the slit.

5.2 *Flat Fields*

Once the object frame has been "sky subtracted" it is "flat fielded". Since the infrared sky spectrum contains many strong features, observation of a "white spot" attached to the interior of the dome is the most effective manner to create a flat field. We have found <1% difference between flats taken at different wavelengths, so usually the dome is measured around 3.3 μm, since the thermal background provides approximately half-full-well ($\sim$ 10,000 ADU) in a few seconds with any of the available gratings, thereby eliminating the need for a dark-current correction (<10 ADU in a few seconds). The image of the slit from one of the two back-to-back gratings is typically shifted by a few pixels with respect to the other, so flats are generally taken with each grating.

Many frames of the "white spot" are taken. These are averaged together after iteratively rejecting bad pixels or medianed to produce a final flat for each grating. The flats are then normalized to unity (generally using IRAF routines such as "response") and divided into the sky-subtracted data frames. Any spectral structure introduced in the data by the white spot or its illumination will be removed by dividing the spectra by the spectrum of a standard star, which is also necessary to remove any atmospheric features (see next section).

5.3 *Atmospheric Absorption Corrections*

The flattened data can generally be treated as any other long-slit spectroscopic image. However, strong atmospheric absorption features are often present in the data. Such absorptions are particularly evident near the edges of the atmospheric windows, e.g., the strong CO_2 absorp-

tions that bracket the He I line near 2.06 μm (other examples can be found by perusing Hall 1970).

Observations of hot stars provide reasonably featureless continua with which to remove these strong atmospheric features (although obvious caution should be used when working around hydrogen recombination lines that often appear in early type stellar spectra). The measurements of the reference stars should be taken at an air mass similar to that of the object spectra. In the most critical cases, such as measurements of the He I 2.06-μm line or the CO 2.3-μm bandheads, repeated measurements of nearby reference stars are often required, since noticeable changes in the absorption strengths have been observed that were not simply correlated with air mass or time.

6. Performance

6.1 *Detector Characteristics*

The characteristics of the SBRC InSb DRO arrays have been described extensively in the literature (e.g., Fowler *et al.* 1987). Table 3 summarizes the detector parameters. The specific detector installed in the IRS has a fairly large number of dead pixels, and some columns exhibit a higher or less-stable dark current. Since the optics limit the field of view to an approximately 6-mm slit length (~ 14 pixels), it has been possible to avoid most of the bad pixels. The low effective read noise of the array is due to the multisampling algorithm described by Fowler and Gatley (1990).

6.2 *Optical Performance*

The reflective optics were designed to produce a blur circle much smaller than the original detector element and, therefore, they perform well with the SBRC array and its smaller pixels. The coma from the collimator alone contributes less than 10 microns blur to the image at the end of the 6 mm slit. The dominant aberration in the spectrometer overall is coma arising in the camera, about 30 microns blur at the edge of the detector. The observed instrument performance is consistent with these figures.

The high sensitivity of the new detector makes the instrument vulnerable to light leaks from the warm walls of the dewar. The use of a double shield is a good strategy for dealing with this problem. Unfortunately, in designing the cable installation for the new array, a large opening was left in the outer shield and small leaks through the inner shield have been difficult to patch. The blanked-off radiation level in the dewar has been reduced to 30–60 photoevents pixel^{-1} sec^{-1}. Note that this is still considerably in excess of the intrinsic dark current at the current operating temperature but comparable to or less than the sky background for most circumstances.

TABLE 3

Device Characteristic for SBRC FPA #136 InSb 58X62 Array

Geometry	58X62 pixels on 76 micron square array, >90% fill-factor
Well capacity	7x10^5 electrons/pixel
Gain	25 electrons/ADU
Readout noise	~80 electrons rms[a]
Dark Current	< 10 electrons/sec/pixel @32 K
Quantum Efficiency	0.7 (typ.)
Non-linearity	< 2% at 50% of full well

[a]With 32 co-adds (see Fowler and Gatley 1990); ~400 electrons rms for single frame

6.3 *Sensitivity and Spectrophotometric Performance*

Table 4 gives the measured sensitivity of the IRS on the 1.5-m telescope at three sample resolutions at various wavelengths. Results for the 4-m telescope and at other resolutions can be calculated by scaling with the appropriate factor (i.e., ~ 2 mag more sensitive on the 4-m telescope for the same resolution and slit size). These values can vary by ±0.5 mag due to variations in emission from the sky and telescope. Because of the low read noise of the SBRC InSb array (~ 80 electrons; see Table 3) the IRS is photon-noise limited at most wavelengths and available resolutions in a few-minute integration.

The IRS also gives superb spectrophotometric results. With a 2″ slit, the normal choice on the 4-m telescope, we have experienced no difficulty obtaining ~ 5% accuracy during photometric nights with typical seeing (in part due to the seeing in the infrared being generally better than in the optical, so that 1″ FWHM or smaller stellar images are common). On the 1.5-m telescope with larger slit widths the spectrophotometric performance is often limited by flat-field accuracy and device stability to ~ 1%.

6.4 *Cryogenic Performance*

The cold optical components require over 24 hours to reach a low-enough temperature that emission is negligi-

TABLE 4

IRS Sensitivity in Magnitudes
S/N ~5 in 1 hour on the 1.5 m telescope

Resolution ($\lambda/\Delta\lambda$)	Wavelength (μm) 1.0	1.25	1.65	2.20
150	15.8	15.9	15.1	14.3
650	15.0	15.1	14.3	13.5
3000	14.4	14.3	13.5	12.7

ble. There appears to be some decrease in the "dark" during an additional 12 hours. The culprit is almost certainly the gratings which are relatively massive and cooled only through the ball bearings on the grating table axis. Once the dewar has been precooled to liquid-nitrogen temperature (in about 6 hours the work surface itself reaches that temperature), the cryocooler cools the detector to its operating point in about 2 hours. The dewar flasks hold 3 and 5 liters, respectively, outer and inner. The hold time of the outer dewar is about 24 hours; the inner will hold almost indefinitely.

Once a thermal steady state has been reached, the temperature of the detector, controlled by a simple proportional controller and measured by the on-chip diode, exhibits a peak-to-peak drift of about 8 mK. Short (10–100 ms) transients in the chip temperature (0.2–0.4 mK) are observed during the integrate and read cycle of the chip. Changing operating modes of the chip, integration times, etc. produces some changes in the control power (and presumably temperature gradients in the chip) but a negligible shift in the operating point. Modulation of the chip temperature due to heating pulsations from the cryocooler is less than 0.5 mK at all harmonics of the coldhead frequency.

7. Sample Spectra

The IRS is a flexible instrument capable of a wide variety of scientific investigations; it is available at the CTIO 4-m and 1.5-m telescopes. Figures 4–7 show examples of the data that can be obtained. Figure 4 shows a moderate-resolution ($\lambda/\Delta\lambda \sim 650$) spectrum of the QSO PG 1416−129 around 2.15 μm. The spectrum, which shows no line emission but clearly detects the continuum, was obtained in ~ 1 hour of real time on the CTIO 1.5-m telescope. Figure 5 is a spectrum of the same object but taken at the CTIO 4-m telescope at a resolution of ~ 150 in ~ 10 minutes. The increase in *S/N* between Figure 4 and Figure 5 is as expected for a larger telescope and

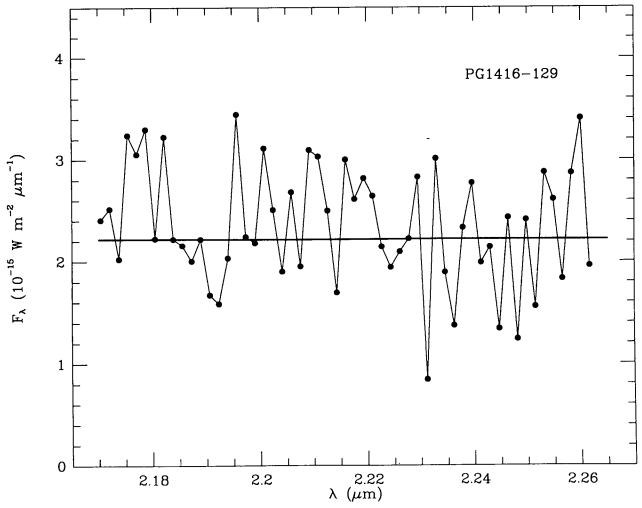

FIG. 4–Spectrum of the QSO PG 1416−129 around 2.15 μm taken at the CTIO 1.5 m with a resolution ($\lambda/\Delta\lambda$) ~ 650. The total time for the observation was ~ 1 hour. No line emission was seen, but the continuum was detected with a $S/N \gtrsim 5$ per pixel. The thick solid line is a linear fit to the data that corresponds to $K \sim 13.2$.

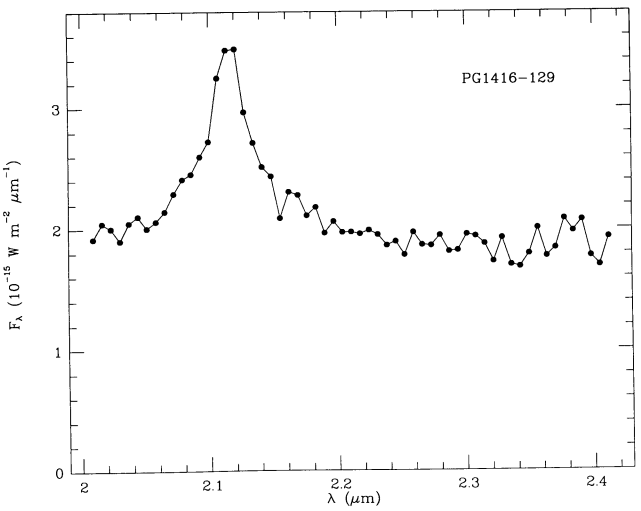

FIG. 5–Another spectrum of PG 1416−129 in the *K* window taken at the CTIO 4-m with a resolution of ~ 160 in ~ 10 minutes. The spectrum shows the expected increase in *S/N* for a larger telescope and lower resolution.

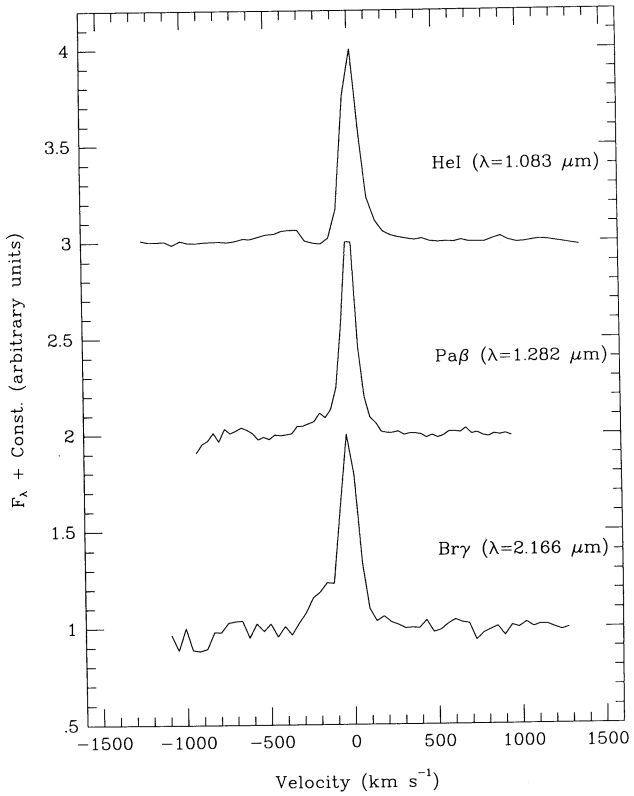

FIG. 6–He I (λ = 1.0830 μm), Pβ (λ = 1.2818 μm), and Bγ (λ = 2.1656 μm) spectra of the symbiotic star BI Cru. Optical line profiles are similar to the He I profile with pronounced P Cygni structure and broad wings. The observations were made with the CTIO 1.5 m at a velocity resolution of ~ 90 km s^{-1} ($\lambda/\Delta\lambda \sim 3300$).

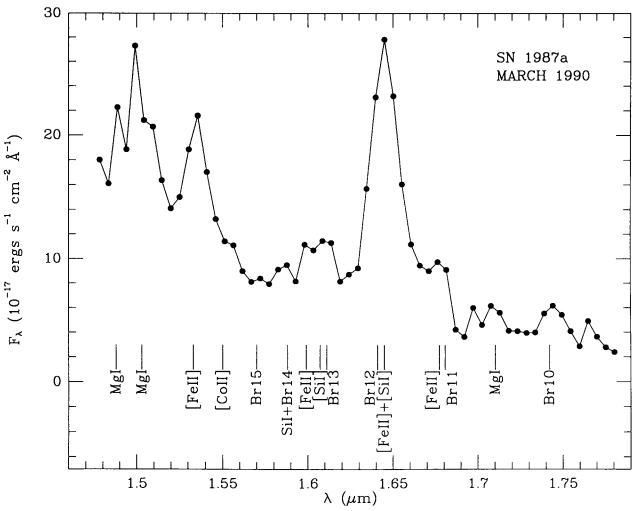

FIG. 7–Low-resolution ($\lambda/\Delta\lambda \sim 150$) *H*-band spectrum of SN 1987A. Many prominent lines are marked. At the time of the observations, made on the CTIO 4-m telescope in March 1990, the supernova had *H* magnitude ~ 14.5, which clearly is composed predominantly of line emission.

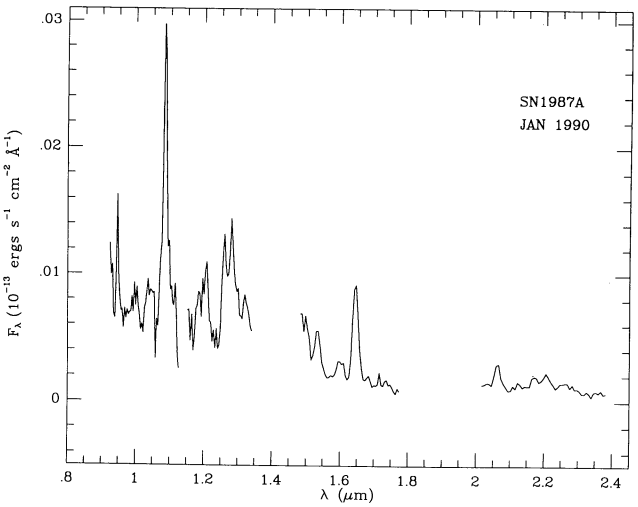

FIG. 8–Low-resolution ($\lambda/\Delta\lambda \sim 150$) spectrum of SN 1987A from 0.9 μm to 2.5 μm. This is a composite of four grating positions.

lower resolution. Figure 6 gives several spectra of the symbiotic star BI Crucis at the highest resolution available ($\lambda/\Delta\lambda \sim 3300$); obvious changes in the line profiles are seen versus wavelength. In particular, the Brackett-γ line shows emission where the He I line is in absorption. Figures 7 and 8 show spectra of SN 1987A taken at the 4-m at low resolution. Figure 7 is an H-band spectrum showing many lines from March 1990, and Figure 8 is a composite of four grating positions showing the spectrum of SN 1987A from 0.9 μm to 2.5 μm from January 1990. Careful comparison of the H-band spectra reveal significant changes in the strengths of the emission lines.

The original construction and recent modification of the IRS involved a large team of people beyond those included in the author list. The superb group of draftsmen and instrument makers at Cerro Tololo who documented and fabricated the entire instrument in-house deserve special mention. Gary Webb and Kim Gillies (NOAO/Tucson) wrote essential software and the entire IR R&D group in Tucson contributed immensely. Gustavo Arriagada, Ramón Galvez, and the CTIO Mountain Staff have provided their usual superb support services. Tirza Del Amo graciously typed the manuscript of this paper.

REFERENCES

Fowler, A. M., and Gatley, I. 1990, *Ap. J. (Letters)*, **353**, L33.
Fowler, A. M., Gatley, I., Stuart, F., Joyce, R. R., and Probst, R. G. 1988, *Proc. SPIE*, **972**, 107.
Fowler, A. M., Probst, R. G., Britt, J. P., Joyce, R. R., and Gillett, F. C. 1987, *Opt. Eng.*, **26**, 3.
Gatley, I., DePoy, D. L., and Fowler, A. 1988, *Science*, **242**, 1217.
Hall, D. N. B., 1970, *Contrib. KPNO*, No. 556.
Zizzo, A. F., and Slaughter, C. D. 1986, *Proc. SPIE*, **627**, 463.